A Journal of

EurJIC

European Journal of Inorganic Chemistry

ChemPubSoc Europe

Accepted Article

Title: Selective displacement of a scorpionand triazole ligand from metallo-cyclam complexes visualised using NMR spectroscopy

Authors: Joseph Wong, Nicholas Proschogo, Matthew Todd, and Peter J. Rutledge

To be cited as: *Eur. J. Inorg. Chem.* 10.1002/ejic.201601474

Link to VoR: http://dx.doi.org/10.1002/ejic.201601474

WILEY-VCH

Selective displacement of a scorpionand triazole ligand from metallo-cyclam complexes visualised using NMR spectroscopy.

Joseph K.-H. Wong, Nicholas Proschogo, Matthew H. Todd* and Peter J. Rutledge*

School of Chemistry, The University of Sydney, Sydney, New South Wales 2006, Australia

* Corresponding authors: Dr Peter J. Rutledge, peter.rutledge@sydney.edu.au, +61 2 9351 5020 and Dr Matthew H. Todd, matthew.todd@sydney.edu.au, +61 2 9351 2180.

Abstract

Target-activated metal complexes (TAMCs) – complexes that remain benign until reaching a specific biomolecular target, binding to which then affects structural change that turns on cytotoxicity or other activity – hold considerable allure. The successful development of TAMCs requires analytical methods that allow clear and unequivocal visualisation of changes in the coordination geometry of these systems in solution. Towards this goal, we report an NMR-based method to monitor coordination/ de-coordination of a pendant triazole ligand to/ from metal-cyclam complexes of zinc(II) and mercury(II). This scorpionand ligand can be displaced from the metal, which remains bound to the macrocyclic ligand, using an appropriate competing ligand: chloride for the mercury(II) complexes, piperidine or citrate at zinc(II). Triazole displacement may be visualised by monitoring the ^{1}H NMR resonance of the single triazole C–H proton environment. Using ^{2}H NMR with a specifically deuterated complex enables the same change to be monitored in a noisy ^{1}H landscape, as would be encountered at a protein binding site or other biological context. MALDI-TOF mass spectrometry experiments provide confirmation that the changes observed by NMR spectroscopy are due to changes in triazole coordination, rather than stripping of the metal ion from the complex.

Keywords

azamacrocycles; click chemistry; scorpiand; scorpionand complexes; target activation

Introduction

Metal complexes have become an increasingly important part of modern medicine as imaging agents and chemotherapeutics.[1-6] However the modes by which metal complexes interact with biological systems are often non-specific, leading to serious side effects in the therapeutic setting and limiting their use.[7] 'Target-activated' metal complexes are thus an enticing prospect: complexes that remain benign and unreactive until reaching their specific biomolecular target, whereupon binding renders structural and functional change in the complex to turn on cytotoxicity or other activity (**Figure 1a**).[8, 9]

While no such 'target-activated' complexes have yet been reported, we have previously described the prototype biotinylated cyclam-Cu^{II} complex **1** and its target-activated behaviour upon interacting with avidin (**Figure 1b**).[8] When the biotin component of **1** interacts with avidin, a change in the geometry of the metal ion is triggered, which can be observed using EPR and ENDOR spectroscopy; *i.e.* the biotin-avidin binding event can be monitored by following changes to the coordination sphere of cyclam-bound Cu^{II}.

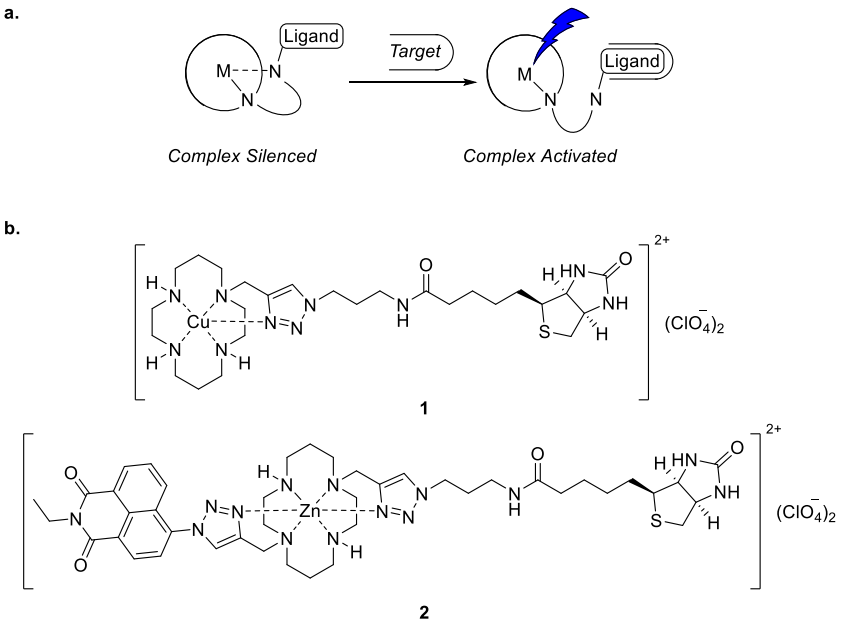

Figure 1: a. The concept of a 'target-activated' metal complex (TAMC): a metal complex that is benign and unreactive until it binds to a specific biomolecular target, which effects a structural change in the complex to turn on activity (represented by the blue lightning bolt). **b.** Structures of biotinylated cyclam complexes previously used to study 'target activated' behaviour: triazole coordination to Cu^{II} in complex **1** was visualised using EPR and ENDOR spectroscopy,[8] while the naphthalimide fluorophore in Zn^{II} complex **2** enabled characterisation of biotin:avidin binding using fluorescence spectroscopy.[9]

The behaviour of such cyclam-triazole-biotin conjugates was further characterised using fluorescence, by incorporating a naphthalimide fluorophore as well as biotin in the 1,8-

disubstituted cyclam conjugate **2**.[9] Significant quenching of the fluorescence emission of Zn^{II} complex **2** was observed at up to 4:1 ratio of **2**:avidin (**Figure 2**). This quenching is quantitatively associated with the biotin-avidin binding event. The observed fluorescence changes are consistent with altered coordination of the biotinylated triazole to Zn^{II} affecting the fluorescence mechanisms in operation.

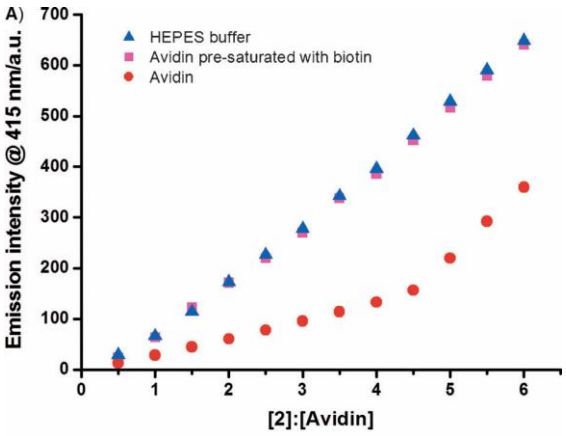

Figure 2: Fluorescence response of **2** in response to the addition of avidin or controls. (Reprinted with permission from *ChemBioChem* **2013**, *14* (2), 224–229. Copyright © 2013 WILEY-VCH)

However the EPR/ENDOR approach was hampered by the poor signal to noise ratio of these spectroscopic techniques and the consequent low resolution of the data obtained, while the fluorescence strategy does not directly visualise metal coordination, so does not specifically elucidate changes in coordination environment. To create and definitively characterise a target-activated metal complex, we need an analytical method that enables unequivocal visualisation of changes in the coordination geometry in these systems.

In separate fluorescence studies of coumarin-substituted cyclam chemosensors for Cu^{II} and Hg^{II}, it was observed that adding certain anions to the mercury complex **3** brought about a revival of the quenched fluorescence.[10] Further investigation revealed that the addition of chloride to mercury complex **3** triggered displacement of the pendant triazole from the metal ion, which remained bound to the macrocycle, whereas adding thiosulphate anion caused demetallation of the same cyclam complex (**Figure 3a**).

Can we use chloride and related species to selectively displace just the triazole from the metal in complexes such as **4**, **5** and **6** (**Figure 3b**), and monitor changes in the triazole environment by NMR spectroscopy? This would then serve as a reference system and enable the direct visualisation of changes in coordination geometry as is required to definitively characterise these scorpionand-triazole systems as target-activated metal complexes. NMR spectroscopy

could provide a more versatile and operationally simple method to further study the metal coordination geometry in cyclam conjugates upon ligand-biomolecule binding, and thus enable validation of the proposed target-activated 'allosteric scorpionand' mechanism that is thought to operate with complexes **1** and **2**.[8, 9]

Herein we report the synthesis of metal-cyclam complexes **4**, **5** and **6** as model systems to evaluate the potential of NMR spectroscopy for visualising biological binding events, and experiments to achieve and characterise anion- and ligand-induced triazole displacement. Triazole-deuterated versions of **4** and **6** were also synthesised for ^{2}H NMR spectroscopic evaluation.

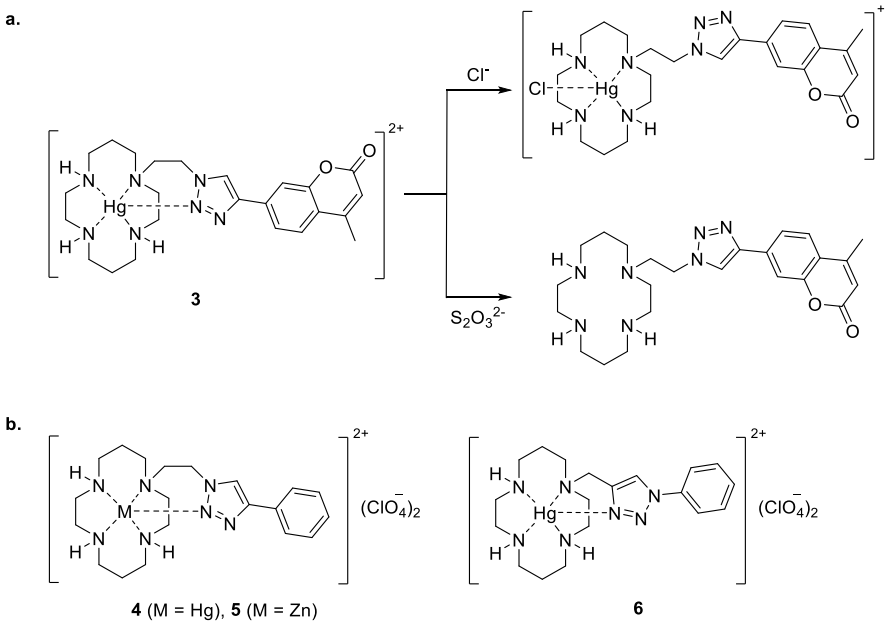

Figure 3: a. The anion induced displacement of triazole or demetallation of **3** reported previously;[10] **b.** structures of metal-cyclam complexes **4**, **5** and **6** used in this study.

Results and Discussion

Synthesis of Ligands and Metal Complexes

The synthetic route to the required phenyl-triazolyl-cyclam ligands **7** and **8** and metal complexes **4**–**6** was adapted from published methods, proceeding from tri-Boc-cyclam **9**, via the tri-Boc-azidoethyl-cyclam **10** or tri-Boc-propargyl-cyclam **11** as precursors for the copper-catalysed azide/ alkyne cycloaddition (CuAAC) or 'click' reaction (**Scheme 1**).[10-13]

For the synthesis of the complexes **4** and **5**, in which the pendant phenyl group is connected via the triazole *C*4, 2-azidoethyl toluenesulfonate **12** was obtained by first refluxing 2-bromoethanol with NaN_3 in H_2O in moderate yield (51%), then used to alkylate tri-Boc cyclam **9** to give tri-Boc-azidoethyl-cyclam **10** in good yield (67%).[10] An alternative route

from **9** to **10** was also explored, via alkylation of **9** with bromoacetonitrile, reduction of the nitrile, and diazotransfer to the resulting amine (**Scheme 1 and Scheme S1**, Supporting Information); this route proved inferior, and is discussed in more detail in the Supporting Information. The azide **10** was reacted with phenylacetylene under the modified click conditions reported previously,[14-16] to afford the Boc-protected ligand **13** in good yield (68%). HCl-mediated Boc-deprotection gave the HCl salt of **7** which was neutralised with excess Ambersep® 900 hydroxide form resin in ethanol to give the cyclam-phenyl ligand **7** in quantitative yield. Adapting a method reported previously for related systems,[17-19] stirring with mercury or zinc perchlorate under room temperature followed by filtration afforded the metal complexes **4** and **5** in good yields (69% and 57% respectively).

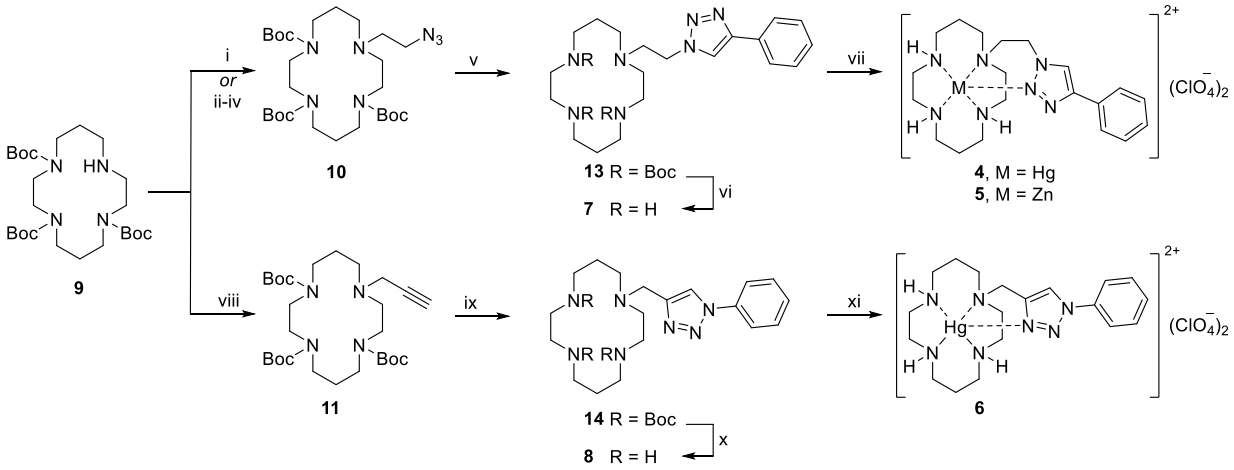

Scheme 1: Synthesis of the complexes **4** and **5** containing the 'reversed' *C*4-phenyl triazole connectivity and mercury complex **6** containing the *N*1-phenyl triazole connectivity: (i) 2-azidoethyl toluenesulfonate **12**, K_2CO_3, MeCN, reflux, 72 h, 67%; (ii) $BrCH_2CN$, K_2CO_3, MeCN, 50 ºC, 16 h, 92%; (iii) H_2, Raney-Ni, NH_3 in EtOH, rt, 48 h, 54%; (iv) 1H-imidazole-1-sulfonyl azide, K_2CO_3, $CuSO_4{\cdot}5H_2O$, MeOH, rt, 16 h, 57%; (v) PhC≡CH, $CuSO_4{\cdot}5H_2O$, sodium ascorbate, THF/H_2O (7:3), 50 °C, 16 h, 68%; (vi) a) HCl, dioxane, rt, 16 h, b) Ambersep® 900 hydroxide form resin, MeOH, rt, 10 min, 99%; (vii) $M(ClO_4)_2{\cdot}xH_2O$, EtOH, rt, 16 h, **4**: 69%, **5**: 57%; (viii) propargyl bromide, K_2CO_3, MeCN, 86%; (ix) PhN_3, $CuSO_4{\cdot}5H_2O$, sodium ascorbate, THF/H_2O (7:3), 50 °C, 16 h, 88%; (x) a) HCl, dioxane, rt, 16 h, b) Ambersep® 900 hydroxide form resin, MeOH, 100%; (xi) $Hg(ClO_4)_2{\cdot}4H_2O$, EtOH, rt, 16 h, 75%.

An analogous approach was followed to synthesise the mercury complex **6** which contains the *N*1 triazole connectivity to the phenyl group (**Scheme 1**). Tri-Boc cyclam **9** was alkylated with propargyl bromide to give tri-Boc-propargyl-cyclam **11** in excellent yield (86%), and this was reacted with phenyl azide to give the Boc-protected ligand **14** in very good yield (88%). HCl-mediated deprotection followed by neutralisation with Ambersep® 900 hydroxide form resin afforded ligand **8** in quantitative yield. Complexation of **8** with mercury perchlorate was initially attempted at 50 ºC to ensure complete reaction; however, droplets of

elemental mercury were observed, likely arising from the decomposition of the mercury perchlorate at the elevated temperature, and the resulting mixture could not be purified. Complexation at room temperature was successful and gave the mercury complex **6** in good yield (75%).

Additional NMR experiments were devised using ^{2}H NMR spectroscopy to enable easier monitoring in biological systems, where it is anticipated that overlap with protein-derived ^{1}H signals may obscure the key triazole proton signal. Given the low natural abundance of deuterium, deuteration of the triazole would provide a highly selective method to visualise changes in triazole environment. Two methods were considered for the synthesis of deuterated triazoles, both of which avoid the need to synthesise new intermediates or starting materials. The first route would see lithiation of the triazole in protected ligands **13** and **14**, followed by D_2O quench; the second approach was to replace the H_2O component of the solvent mixture used for the CuAAC reaction with D_2O so that the final protonation[20] step in the mechanism delivers ^{2}H in place of ^{1}H. By virtue of its simplicity and mild reaction conditions the second option was preferred; this protocol adapts the procedure reported by Akula and Lakshaman who have synthesised deuterated triazoles in a biphasic system.[21]

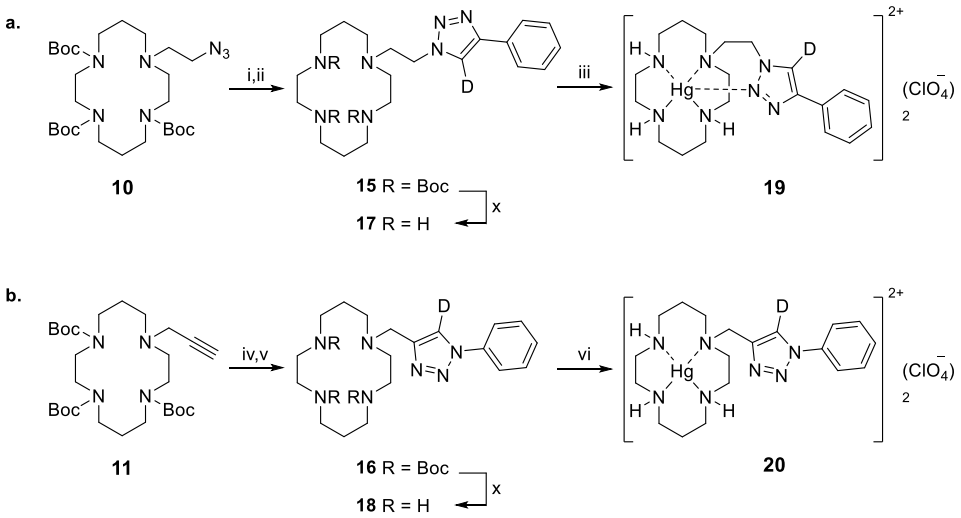

Scheme 2: Synthesis of the deuterated complexes **19** and **20**. **a.** Complex **19** containing the *C*4-phenyl triazole connectivity: (i) PhC≡CH, $CuSO_4{\cdot}5H_2O$, sodium ascorbate, THF/D_2O (7:3), 50 °C, 16 h, 82%; (ii) a) HCl, dioxane, rt, 16 h, b) Ambersep® 900 hydroxide form resin, MeOH, rt, 10 min, 67%; (iii) $Hg(ClO_4)_2{\cdot}4H_2O$, EtOH, rt, 16 h, 34%. **b.** Complex **20** containing the *N*1-phenyl triazole connectivity: (iv) PhN_3, $CuSO_4{\cdot}5H_2O$, sodium ascorbate, THF/D_2O (7:3), 50 °C, 16 h, 78%; (v) a) HCl, dioxane, rt, 16 h, b) Ambersep® 900 hydroxide form resin, MeOH, rt, 10 min, 100%.; (vi) $Hg(ClO_4)_2{\cdot}4H_2O$, EtOH, rt, 16 h, 31%.

Thus click precursors **10** and **11** were combined with their corresponding coupling partners, phenyl azide and phenylacetylene, under the same click conditions but using a THF/D_2O solvent system (**Scheme 2**). These reactions proceeded in very good yields (82% and 79%

respectively) and deuterium incorporation (90% and 92% *D*-incorporation, determined by HRMS) to give Boc-protected ligands **15** and **16**. Acid-mediated Boc-deprotection gave the deuterated ligands **17** and **18** in good (67%) and quantitative yield respectively. Complexation of these ligands with mercury perchlorate afforded the deuterated complexes **19** and **20** in poor but tolerable yields (34% and 31% respectively). HRMS analysis indicated low levels of deuterium leakage during the conversion of **15** and **16** to metal complexes **19** and **20**, which retain ≥80% *D*-incorporation following the deprotection and metalation steps.

Visualisation of Triazole Displacement by NMR Spectroscopy

Control Experiments with Free Ligands

To establish a baseline for the analysis of these complexes, the free ligands **7** and **8** were subjected to the high concentrations of chloride needed to induce triazole displacement. Thus each ligand was dissolved in D_2O and titrated with NaCl (in D_2O) in the NMR tube.

For the titration of the *C*4 ligand **7** (**Figure S3**, Supporting Information), as the concentration of Cl^- was increased, all of the peaks of **7** gradually moved slightly downfield, to a final change of *ca.* 0.1 ppm after the addition of 100 equivalents of Cl^-; no changes to individual peak shapes or multiplicities were evident. For the titration of the *N*1 ligand **8** (**Figure S4,** Supporting Information), as the concentration of Cl^- increased, the majority of peaks gradually moved very slightly downfield, to a final change of *ca.* 0.03 ppm after the addition of 100 equivalents of Cl^-. One peak moved further: the multiplet at *ca.* 2.80 ppm, which moved downfield to 2.92 after 100 equivalents of Cl^-, and in so doing became deconvoluted from other signals at 2.73 and 2.85 ppm.

*^{1}H NMR Characterisation of Triazole Displacement in Mercury Complex **4***

The ^{1}H NMR spectroscopic titration of the *C*4 Hg^{II} complex **4** revealed important changes upon the addition of Cl^- (**Figure 4** and **Figure S1**). Notably, the peaks in the spectra corresponding to the triazole (8.70) and phenyl group (7.53 to 7.93 ppm) in **4** (**Figure 4, black**) moved upfield with increasing concentration of Cl^-, in contrast to equivalent signals of the control **7** (**Figure S3**). A significant movement of the triazole proton was observed, from 8.70 for the Hg complex **4**, to 8.48 after the addition of 5 equivalents of Cl^-; further addition of Cl^- had a negligible impact on the triazole proton signal, although a small downfield movement of this signal was detected at very high equivalents of Cl^- (> 50 equivalents). That five equivalents of Cl^- are required to move the triazole proton to its point of greatest

difference suggests a competitive equilibrium process for coordination to mercury between the triazole and added Cl^-, rather than direct substitution of the coordinated triazole by Cl^-, which would presumably require only a stoichiometric amount of Cl^-. The observed upfield movement of the triazole proton signal corresponds to an increase in electron density in the triazole-phenyl pendant group, and is thus consistent with displacement of the triazole from the Lewis acidic metal ion. Overall a small upfield movement of *ca.* 0.03 ppm in the phenyl signals was observed after the addition of 100 equivalents of Cl^- (**Figure 4, red**); this comparatively small change was not unexpected as the phenyl group is distant from the mercury coordination site. The positions of the triazole and phenyl peaks in the final spectrum of **4** + 100 equiv. Cl^- (**Figure 4, red**) corresponded closely to those of the control **7** + 100 equiv. Cl^- (**Figure 4, blue**), supporting the hypothesis that the triazole is no longer coordinated to the metal centre.

In contrast, the cyclam-derived signals at ~1.5–4.0 ppm appeared quite differently in these two spectra (**Figure 4, blue and red**). Of the remaining methylene signals, the multiplet at 4.79–4.95 ppm (the upfield portion of the multiplet which is obscured by the residual solvent signal) is due to the linker CH_2 adjacent to the triazole. This signal coalesced into a triplet after 5 equivalents of Cl^- had been added, consistent with greater freedom of movement gained at this position after triazole displacement, which would render these protons equivalent on an NMR time-scale. The remaining upfield peaks ($\delta < 3.6$) correspond to protons of the cyclam CH_2 groups and the linker CH_2 nearest the cyclam in **4**. These signals were complicated, due to the different geometries that cyclam can adopt after metal binding, and the consequent chirality of the coordinating nitrogens.[22] The splitting patterns of these methylenes did change a little at high concentrations of Cl^-, however these peaks remained at essentially the same positions.

Most importantly, this region of the spectrum was clearly very different to the spectrum of the metal-free sample (**Figure 4, blue**), suggesting that the metal ion remained bound to the macrocycle even after addition of 100 equiv. Cl^- (**Figure 4, red**). In comparison with the ^1H NMR spectrum of the free ligand control **7** (**Figure 4, blue**), the cyclam-derived methylene signals in the spectra of both the chloride-free mercury complex **4** (**Figure 4, black**) and **4** + 100 equiv. Cl^- (**Figure 4, red**) appeared significantly downfield (*ca.* 1 ppm). Additionally, in the spectra of the complex **4**, these signals remained convoluted and overlapping after chloride addition, compared to the well resolved methylene signals of **7** + 100 equiv. Cl^-.

This suggests strongly that Hg^{II} remained complexed to cyclam in **4**, even after addition of 100 equiv. Cl^-.

Thus the change in the ^1H NMR shift of the triazole signal from 8.70 to 8.48 ppm, combined with the minimal changes to the methylene signals indicate that (i) mercury remained bound to the cyclam, but (ii) the pendent triazole had been displaced by the addition of Cl^-, and (iii) triazole displacement from the metal manifested in a clearly discernible upfield shift in the ^1H signal due to the triazolyl CH.

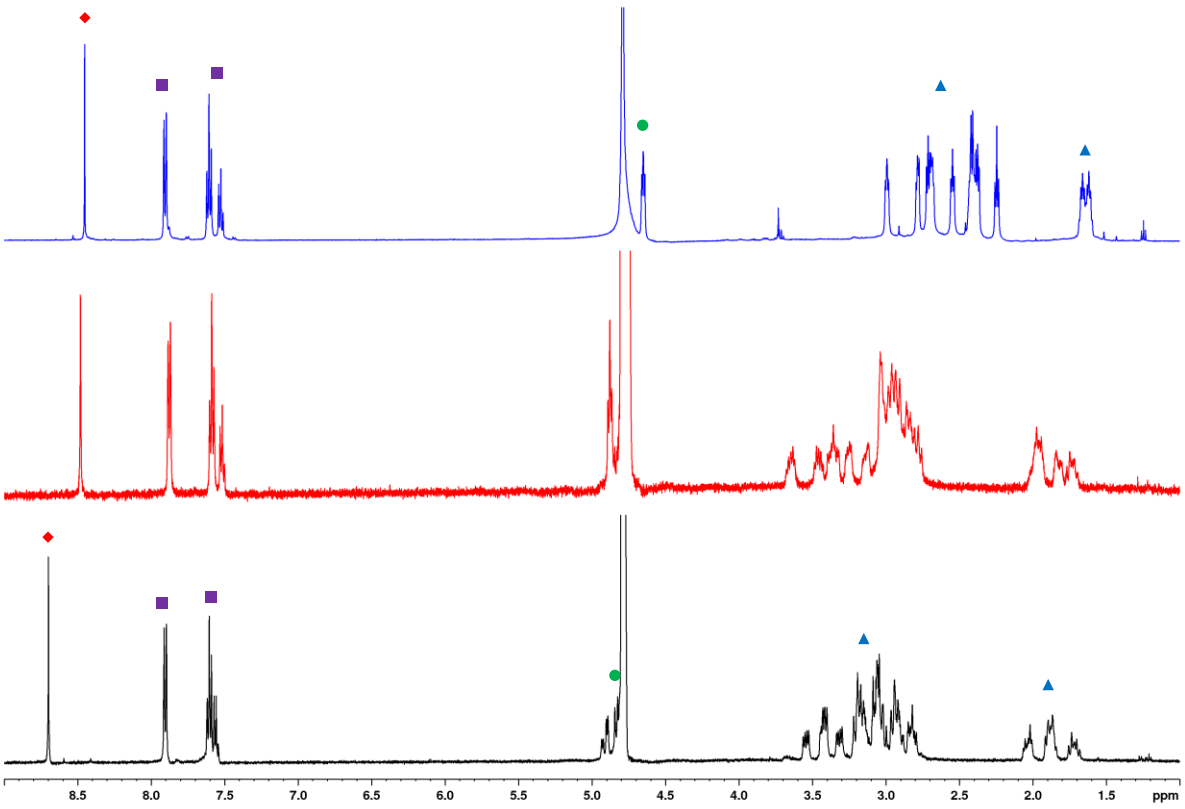

Figure 4: ^1H NMR spectroscopic titration of the *C*4 Hg^{II} complex **4** with Cl^-: free ligand **7** + 100 equiv. Cl^- (Blue), **4** + 100 equiv. Cl^- (Black), **4** (Red); ◆: Triazole C*H*, ■: Phenyl C*H*, ●: Linker CH_2 adjacent to phenyl, ▲: Remaining CH_2.

*^1H NMR Characterisation of Triazole Displacement in Zinc Complex **5***

Initial attempts to effect the displacement of the Zn^{II}-coordinated triazole in the *C*4 complex **5** using anions (Cl^-, SCN^- and $S_2O_3^{2-}$) or imidazole as the competing ligand were unsuccessful, with no significant changes to peak positions observed (**Figure S5**). These negative results were not surprising given that zinc is considered marginally hard, while mercury is a soft metal according to the Hard and Soft Acids and Bases Principle, and the strength of their binding to a variety of ligands differs accordingly.[23] This is apparent in the stability constants for complex formation of Hg^{II} with Cl^- (log $K_1 = 6.7$) compared to those of Zn^{II} with

Cl^- (0.5), SCN^- (0.9), $S_2O_3^{2-}$ (2.3) and imidazole (2.6).[24] The stability constant for complex formation between aqueous Zn^{II} and citrate is 5.0.[24])

Instead displacement of the triazole within complex **5** was achieved using either piperidine or citrate as the competing ligand. In the ^1H NMR spectrum of the Zn^{II} complex **5** (**Figure 5, black**) the triazole proton appeared as several peaks of varying intensity, presumed to arise from the different geometries the macrocycle can adopt after metal binding.[22] (This is a contrast to spectra of Hg^{II} complex **4**, in which the signal due to this proton appeared as a

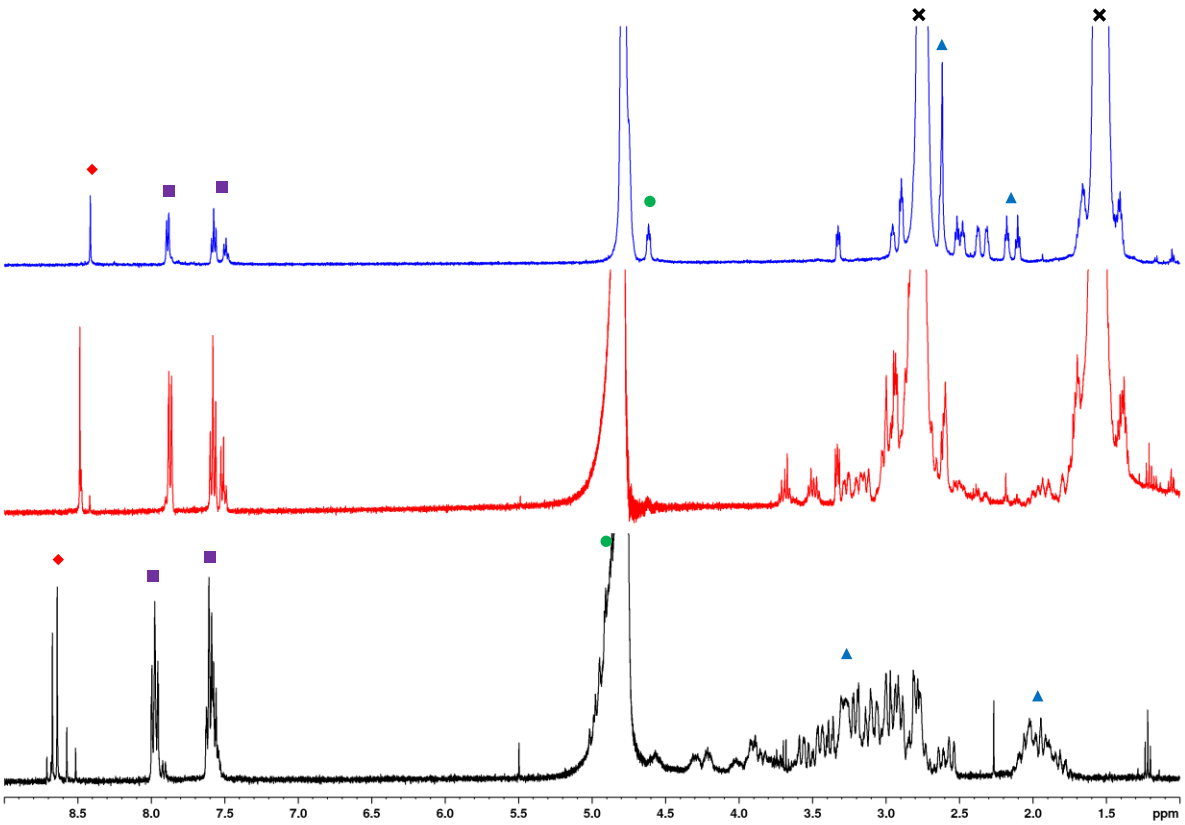

Figure 5: ^1H NMR spectroscopic titration of the *C*4 Zn^{II} complex **5** with piperidine: free ligand **7** + 100 equiv. piperidine (Blue), **5** + 100 equiv. piperidine (Red), **5** (Black); ◆: Triazole C*H*, ■: Phenyl C*H*, ●: Linker CH_2 adjacent to phenyl, ▲: Remaining CH_2, ✖: Piperidine CH_2.

singlet.) After addition of 100 equivalents of piperidine these triazole signals had moved upfield by *ca.* 0.15 ppm, and the two largest peaks at 8.67 and 8.64 ppm coalesced into one major singlet peak at 8.49 (**Figure 5, red**). In the complex **5**, the peaks corresponding to the pendant phenyl group appeared as multiplets in the range 7.50–7.65 and an apparent triplet at 7.98 ppm; after addition of 100 equivalents of piperidine, the multiplets had moved upfield by *ca.* 0.03 ppm and resolve into two distinct triplets at 7.58 and 7.49, while the apparent triplet at 7.98 moved to become an apparent doublet at 7.88 ppm. Of the higher field methylene protons, the peaks corresponding to the linker CH_2 adjacent to the triazole were

obscured by the residual solvent while the various overlapping multiplets due to cyclam-CH_2 groups did not move significantly, even after addition of 100 equivalents of piperidine.

Titration of the Zn^{II} complex **5** with trisodium citrate (**Figure S6**) revealed changes in the peaks consistent with those observed in the piperidine titration, and with the Cl^- titration of the Hg^{II} complex **4**. The two major triazole peaks moved upfield from 8.67 and 8.63 ppm in the spectrum of **5** without added citrate, to 8.58 and 8.50 in the spectrum of **5** + 100 equiv. citrate. Of the peaks corresponding to the pendant phenyl group, the multiplets (7.50–7.65) moved upfield by *ca.* 0.03 ppm, while the previously assigned apparent triplet at 7.97 presented as a double-doublet (**Figure S6, black**), but became an apparent triplet at 7.89 after the addition of 100 equivalents of citrate (**Figure S6, red**).

As in the piperidine experiment, the peak corresponding to the linker CH_2 adjacent to the triazole was obscured by the residual solvent signal and the complex signals arising from cyclam environments remained significantly different to the spectrum of the free ligand **7**, after the addition of 100 equivalents of citrate.

*^{1}H NMR Characterisation of Triazole Displacement in Mercury Complex **6***

Ligand **8** (phenyl group at *N*1, cyclam at *C*4, 1 CH_2 group between cyclam and triazole) has the opposite triazole connectivity to **7** (phenyl group at *C*4, cyclam at *N*1, 2 CH_2 groups between cyclam and triazole), and thus presents a subtly different coordination environment to a ligating metal ion (**Figure 3**). As a consequence, the ^{1}H NMR titration of mercury complex **6** with increasing concentrations of Cl^- (**Figure S7**) was less clear cut.

The change in the position of the signal due to the triazole proton was noticeably less pronounced than with complex **4**: this signal comes at 8.70 ppm for the *N*1 complex **6** (**Figure S7, black**) and moves upfield to 8.63 after the addition of 100 equivalents of Cl^- (**Figure S7, red**), a change of only 0.07 ppm. Contrast this to the response of the *C*4 complex **4**, in which this proton moved by 0.22 ppm after only 5 equivalents of Cl^- were added. While the triazolyl and phenyl protons of the *N*1 complex **6** moved upfield as Cl^- was added, there remained a significant difference between the position of these shifts in the spectra of **6** + 100 equiv. Cl^- (**Figure S7, red**) and of the control **8** + 100 equiv. Cl^- (**Figure S7, blue**).

The two doublets of the *N*1 complex **6** at 3.89 and 4.37 ppm – each due to one proton in the CH_2 linker between cyclam and triazole – coalesced at 4.27 after the addition of 100 equiv. of Cl^-, mirroring the behaviour of the C*H*$_2$-triazole signals of the *C*4 complex **4**. The remaining

peaks (δ < 3.5) correspond to the cyclam CH_2 groups and displayed complex changes to splitting patterns while remaining at the same chemical shifts throughout the titration, as seen with the *C*4 complex **4**.

Overall this NMR titration did not deliver unequivocal evidence that the addition of Cl^- to the mercury complex **6** displaces the coordinated triazole. More significantly, it does not offer a clear means to monitor triazole displacement by NMR spectroscopy. Consequently, further investigations focused on the *C*4 connectivity, with Hg^{II} complex **4**, Zn^{II} complex **5**, and deuterated Hg^{II} complex **15**.

Visualisation of Triazole Displacement by ^2H NMR

Having ascertained using ^1H NMR that chloride-mediated triazole displacement from complex **4** manifests in a 0.22 ppm shift in the triazole CH signal, we wished to confirm that a similar change occurs in the corresponding deuterated complex **19**. Comparing the ^2H NMR spectrum of **19** + 100 equiv. Cl^- (**Figure 6, red**) with the spectrum of complex **19** (**Figure 6, black**), it was evident that the deutero-triazole C–D signal had undergone a corresponding shift upfield, from 8.69 to 8.49 ppm after the addition of 100 equiv. of Cl^-.

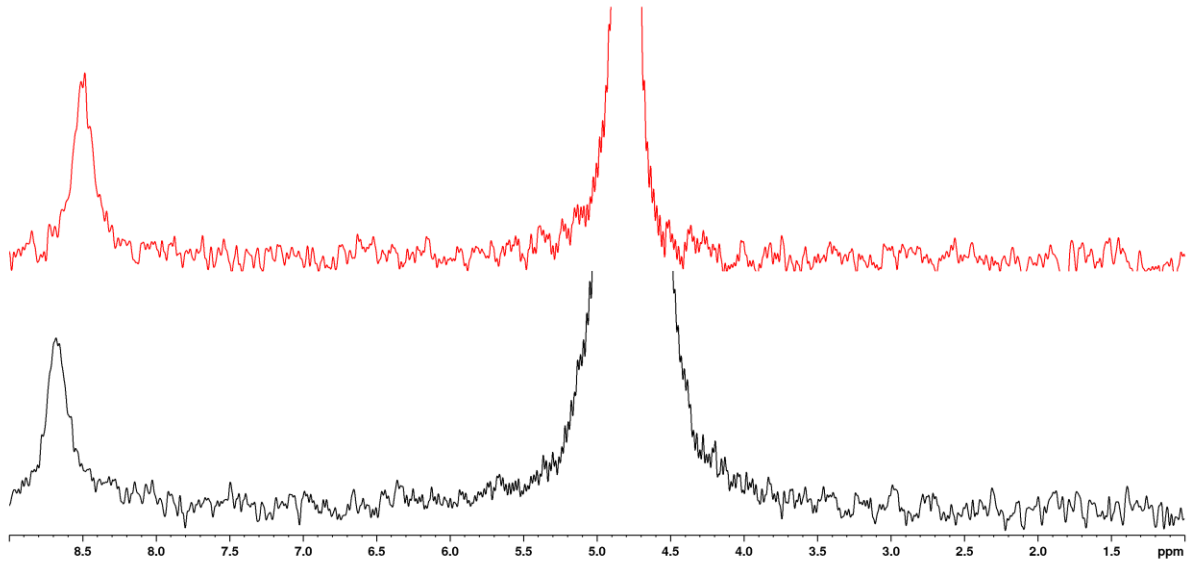

Figure 6: ^2H NMR spectra of: **19** + 100 equiv. Cl^- (red), **19** (black); spectra obtained in H_2O with D_2O as reference.

These ^2H chemical shifts are in excellent agreement with those seen in the ^1H NMR spectra: 8.69 *vs.* 8.70 for the complexes, 8.49 *vs.* 8.48 for the complexes after Cl^- addition. Given this close correspondence with the ^1H NMR results, and the ease in which the deuterated triazoles were generated, ^2H NMR offers a useful complement to the ^1H NMR investigation in more

complicated systems, such as biotin-avidin binding and other ligand-biomolecule interactions.

Mass Spectrometric (MS) Investigations

To validate conclusions drawn from the NMR experiments – i.e. that the added competing species (chloride, piperidine or citrate) displace the triazole from the metal in these complexes without disrupting metal:cyclam ligation – mass spectra were recorded for complexes **4**, **5** and **6** in the absence and presence of added competing species.

Initial experiments using electrospray ionisation (ESI) MS were unsuccessful, on account of two complicating factors. First, the conditions employed triggered a significant degree of metal displacement from both of the *C*4-linked complexes **4** and **5**: the base peak in the spectra of both complexes (**Figures S8** and **S9**)was the signal at *m/z* 372.2 corresponding to the demetallated ligand [**7**+H]$^+$. Secondly, some of the ClO_4^- counterions of complexes **4**, **5** and **6** were reduced under ESI conditions, generating Cl^- and thence forming chloride adducts of these metal complexes even in the absence of extraneous chloride. For *C*4 Hg^{II} complex **4**, a set of peaks centred at *m/z* 608.2 showed the characteristic isotope pattern for mercury and correspond to [**4**–2ClO_4+Cl]$^+$ (**Figure S8**); in the ESI spectrum of *C*4 Zn^{II} complex **5**, a signal at *m/z* 470.2 corresponds to Cl^- adduct [**5**–2ClO_4+Cl]$^+$ (**Figure S9**); with *N*1 Hg^{II} complex **6**, a set of peaks at *m/z* 594.1 are due to Cl^- adduct [**6**–2ClO_4+Cl]$^+$) (**Figure S10**). Attempts to inhibit Cl^- adduct formation by changing ionisation voltages on the spectrometer were not successful.

While ESI is considered a soft ionisation technique, evidently the spectrometer environment is sufficiently high in energy to initiate reactions that disrupt or destroy these coordination complexes, and promote reduction of the ClO_4^- counterion to Cl^-. Colton and Dakternieks previously observed formation of Cl^- adducts from perchlorates under ESI+ MS conditions, during a study of mercury phosphine complexes with perchlorate counterions.[25] In the current context, this outcome presents a problem for our experimental design, given the intended use of Cl^- to displace the triazole from mercury complexes **4** and **6**. Indeed the ESI spectrum of **4** + 100 equiv. Cl^- (**Figure S11**) looks very similar to the spectrum of **4** alone (**Figure S8**), while the spectrum of **6** + 100 equiv. Cl^- (**Figure S12**) is dominated by the demetallated species [**8**+H]$^+$, though there is a cluster of very weak peaks centred at *m/z* 595.1 due to the Cl^- adduct [**6**–2ClO_4+Cl]$^+$. The ESI MS of complex **5** + 100 equiv.

piperidine (**Figure S13**) presents different challenges, as it does not show any ion recognisable as corresponding to the complex **5**, piperidine adducts of **5**, or even the free ligand **8**.

The problems encountered with decomposition of the metal complexes and reduction of perchlorate counterions were overcome by using MALDI-TOF MS. Using α-cyano-4-hydroxycinnamic acid (α-CCA) as the MALDI matrix, the MALDI-TOF MS of the *C*4 Hg^{II} complex **4** (**Figure S14**) showed sets of peaks corresponding to the loss of two perchlorates (*m/z* 572.3, [**4**–$2ClO_4$–H]$^+$) and to loss of one perchlorate (*m/z* 672.2, ([**4**–ClO_4]$^+$); importantly, no Cl^- adducts were observed in the absence of added extraneous chloride.

Upon the addition of 100 equiv. of Cl^- (**Figure S15**), a new set of strong signals corresponding to the Cl^- adduct of complex **4** ([**4**–$2ClO_4$+Cl]$^+$) were apparent at *m/z* 608.2. The original set of peaks at *m/z* 672.2 ([**4**–ClO_4]$^+$) had disappeared, while the signal centred at *m/z* 572.3 ([**4**–$2ClO_4$–H]$^+$)) remained. These two sets of MALDI-TOF data for the complex **4** substantiate the successful Cl-mediated triazole displacement observed in the NMR experiments, and the proposed mechanism involving Cl^- coordination to the Hg^{II} centre while the metal remains bound to cyclam.

In the MALDI-TOF MS of Zn^{II} complex **5** (**Figure S16**), the most important signals were a set of peaks at *m/z* 534.2 ([**5**–ClO_4]$^+$), and an adduct species formed between **5** and the α-CCA matrix at *m/z* 623.3 ([**5**–$2ClO_4$–H+αCCA]$^+$). However, the spectra arising from this complex with added piperidine (100 equiv., **Figures S17** and **S18**) did not provide confirmatory evidence for the **5**:piperidine complex that had been anticipated on the basis of the NMR data.

Working instead with the 2′,4′,6′-trihydroxyacetophenone matrix (THAP), with and without added ammonium citrate, the 'THAP-only' MS of **5** (**Figure S19**) showed signals for [**5**–$2ClO_4$–H]$^+$ at *m/z* 434.3, and [**5**–ClO_4]$^+$ at *m/z* 534.2; there were also a Cl^- adduct [**5**–$2ClO_4$+Cl]$^+$ at *m/z* 470.2, and a matrix adduct [**5**–$2ClO_4$–H+THAP]$^+$ at *m/z* 602.3. In contrast, the MS of **5** run with the THAP matrix and added citrate (**Figure S20**) only held two of these signals: [**5**–$2ClO_4$–H]$^+$at *m/z* 434.2, and the THAP adduct at 602.2. The base peak set in this spectrum was centred at *m/z* 626.1 which corresponds to the dibasic citrate adduct [**5**–$2ClO_4$+H+citrate^{2-}]$^+$. This result confirmed that citrate is able to coordinate to the Zn^{II} complex **5** without displacing it from the macrocycle, and supports the conclusions drawn

from the NMR experiments that citrate displaces the triazole from Zn^{II} in **5** as Cl^- does with the corresponding Hg^{II} complex **4**.

The MALDI-TOF MS spectrum of the *N*1 Hg^{II} complex **6** (**Figure 21**) also showed sets of signals arising from the loss of two perchlorates (*m/z* 558.3 [**6**–2ClO_4–H]$^+$) and loss of one perchlorate (*m/z* 658.2 ([**6**–ClO_4]$^+$), with no evidence of unwanted Cl^- adducts. As was the case in the NMR experiments with complex **6** detailed above, the changes wrought by adding Cl^- to this complex were less clear cut. The MALDI-TOF MS spectrum of **6** + 100 equiv. Cl^- (**Figure S22**) showed a variety of species, but did include peaks that correspond to the Cl^- adduct [**6**–2ClO_4+Cl]$^+$ centred at *m/z* 594.2, corroborating the triazole displacement observed by NMR spectroscopy, along with the original set of peaks for [**6**–2ClO_4–H] at *m/z* 558.2.

Conclusion

These experiments demonstrate that it is possible to displace the triazole ligand from these mercury and zinc complexes without disrupting macrocycle coordination, if the competing ligand is matched to the metal complex. Chloride anion triggers triazole displacement in mercury complexes **4** and (at least partially) **6**, piperidine and citrate do similarly with zinc complex **5**. The resulting displacement can be visualised by a change in the NMR resonance of the triazole C–H (^{1}H NMR) or, in the specifically deuterated analogue **19**, the triazole C–D. Using ^{2}H NMR offers orthogonality for work with biomolecular systems, in which the key triazole ^{1}H signal would likely be obscured by protein or nucleic acid-derived 1H signals. MALDI-TOF mass spectrometry verifies the conclusion that the metal-cyclam complex remains intact after addition of chloride (to **4** and **6**) or citrate to **5**; the **5**:piperidine complex proved more elusive and less stable under the MS conditions investigated.

While spectral changes are observed with all metal complexes tested, the *C*4-linked mercury complex **4** offers the best combination of operational simplicity and clear, discernible change in the key ^{1}H resonance. The triazole proton appears as a distinct singlet in spectra of mercury complex **4** before and throughout titration experiments, and in the free ligand 7; it undergoes an upfield shift of 0.22 ppm upon triazole displacement from the metal. This change is replicated in the ^{2}H spectra and provides a clear reference marker for triazole coordination/ decoordination in subsequent work with ligand/ biomolecule binding events like those detailed in **Figure 1**. The corresponding proton in the *C*4-linked zinc complex **5** undergoes similar change in position and might reasonably be utilised as a marker in a similar

manner. However this proton presents as a comparatively complicated mixture of several signals in spectra of the complex, which brings additional complexity to analysis.

Changes in the spectra of *N*1-linked mercury complex **6** upon addition of Cl^- are less pronounced, such that this system does not enable clear monitoring of triazole displacement by NMR. In discussing differences in the behaviour of the mercury complexes **4** and **6**, it is interesting to consider structural data previously reported for similar complexes. Crystal structures of complexes that include ligands with triazole connectivity as in **4** and **5** (phenyl group at *C*4, cyclam at *N*1) show that the pendant triazole coordinates to the metal through its central nitrogen atom (*N*2) and thus forms a six-membered metallocycle (as shown for **4** and **5** above, **Figure 3**).[10, 16] Whereas in structures of complexes that contain ligands with the triazole connectivity of **6** (phenyl group at *N*1, cyclam at *C*4), the triazole coordinates through nitrogen atom *N*3 (derived originally from the terminal *N* of the azide coupling partner) forming a five-membered metallocycle (as shown for **6** above, **Figure 3**).[8, 16] This difference in chelate size is presumably the reason behind the different response of the triazole to added Cl^- in complexes **4** and **6**.

While the ^{2}H NMR experiments demonstrate the concept of orthogonality designed to simplify detection in biological environments, the inherently low sensitivity of ^{2}H NMR is likely to be problematic with regard to the concentrations of proteins and other biomolecules required for binding studies. To extend this concept, the next step is to prepare selectively fluorinated triazoles,[26, 27] then exploit the improved sensitivity of ^{19}F NMR to advance the method.

In parallel, work is underway to apply this method, using ^{1}H and ^{2}H NMR in the first instance, to characterise the biotin/ avidin couple previously investigated (**Figure 1**). Using both the original and reversed triazole connectivities, the aim is to verify the changes in triazole:metal coordination upon biomolecule binding previously proposed on the basis of EPR/ENDOR and fluorescence experiments. The ultimate goal of this work is to apply insights gleaned from these model studies to the development of target-activated metal complexes for therapeutic applications.

Experimental

Synthetic Procedures

Safety note: *Sodium azide, organic azides and perchlorate salts of metal complexes with organic ligands are potentially explosive. Only small amounts of material should be prepared and these should be handled with caution.*

Tri-tert-butyl 11-(2-(4-phenyl-1H-1,2,3-triazol-1-yl)ethyl)-1,4,8,11-tetraazacyclotetradecane-1,4,8-tricarboxylate ***13***

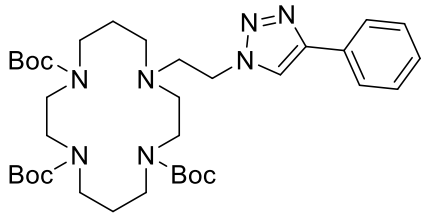

Tri-Boc-azidoethylcyclam **10** (108 mg, 0.19 mmol) and phenylacetylene (25 µL, 0.23 mmol) were reacted using general synthetic procedure A and purified by automated flash column chromatography (10 g cartridge, 30% EtOAc in P.E. over 3 CV, 55% over 2 CV and 84% over 9 CV) to afford click product **13** as a white foam (109 mg, 87%). **^{1}H NMR** ($CDCl_3$, 300 MHz): δ 1.44 (s, 9H), 1.46 (s, 18H), 1.62 – 1.80 (m, 4H), 2.46 – 2.56 (m, 2H), 2.62 – 2.73 (m, 2H), 2.98 (t, 2H, *J* 6.5), 3.09 – 3.38 (m, 12H), 4.41 (t, 2H, *J* 6.6), 7.29 – 7.37 (m, 1H), 7.38 – 7.47 (m, 2H), 7.78 – 7.87 (m, 3H). **LRMS** (ESI+): *m/z* 672.1 ($[M+H]^+$, 13%), 694.2 ($[M+Na]^+$, 100%), 1364.9 ($[2M+Na]^+$, 61%). **HRMS** (ESI+): *m/z* Calcd. for $C_{35}H_{57}N_7NaO_6$+ $[M+Na]^+$ 694.4263, found 694.4261. The spectroscopic data were in agreement with those in the literature.[10]

1-(2-(4-Phenyl-1H-1,2,3-triazol-1-yl)ethyl)-1,4,8,11-tetraazacyclotetradecane ***7***

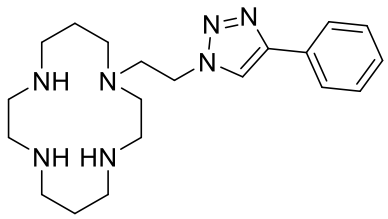

Protected ligand **13** (77 mg, 0.12 mmol) was deprotected using general synthetic procedure C to afford the Boc-deprotected target **7** as a sticky off-white solid (42 mg, 99%). **^{1}H NMR** (D_2O, 500 MHz): δ 1.45 – 1.53 (m, 2H), 1.53 – 1.59 (m, 2H), 2.09 (t, 2H, *J* 6.3), 2.20 (t, 2H,

J 5.5), 2.25 – 2.36 (m, 4H), 2.43 (t, 2H, *J* 5.6), 2.53 (t, 2H, *J* 5.7), 2.54 – 2.64 (m, 4H), 2.88 (t, 2H, *J* 5.2), 4.51 (t, 2H, *J* 5.4), 7.43 (t, 1H, *J* 7.6), 7.51 (t, 2H, *J* 7.6), 7.79 (d, 2H, *J* 7.7), 8.29 (s, 1H). **^{13}C NMR** (D_2O, 75 MHz): δ 25.6, 26.5, 44.2, 45.2, 45.3, 45.6, 45.9, 46.6, 48.4, 50.3, 52, 52.5, 123.1, 125.7, 129.3, 129.6, 129.7, 147.5. **LRMS** (ESI+): *m/z* 372.2 ($[M+H]^+$, 100%). **HRMS** (ESI+): *m/z* Calcd. for $C_{20}H_{34}N_7^+$ 372.2870, found 372.2870. The spectroscopic data were in agreement with those in the literature.[10]

*Mercury perchlorate complex of 1-(2-(4-phenyl-1H-1,2,3-triazol-1-yl)ethyl)-1,4,8,11-tetra-azacyclotetradecane **4***

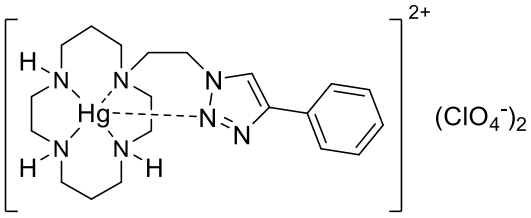

Ligand **7** (66 mg, 0.18 mmol) was complexed with $Hg(ClO_4)_2 \cdot 4H_2O$ (84 mg, 0.18 mmol) at rt using general synthetic procedure E to afford mercury complex **4** as a white solid (94 mg, 69%). **m.p.**: 135 ºC (decomp.). **LRMS** (ESI+): *m/z* 372.2 ($[M–Hg–2ClO_4+H]^+$, 100%), 608.2 ($[M–2ClO_4+Cl]^+$, 50%). **LRMS** (MALDI-TOF, α-CCA): *m/z* 572.3 ($[M–2ClO_4–H]^+$, 100%), 672.2 ($[M–ClO_4]^+$, 13%). **HRMS** (ESI+): *m/z* Calcd. for $C_{20}H_{33}ClHgN_7^+$ $[M–2ClO_4+Cl]^+$ 608.2187, found 608.2190. **FTIR** (ATR) ν_{max}/cm^{-1}: 3265, 1470, 1453, 1076, 930, 884, 842, 770, 699, 621.

*Zinc perchlorate complex of 1-(2-(4-phenyl-1H-1,2,3-triazol-1-yl)ethyl)-1,4,8,11-tetraaza-cyclotetradecane **5***

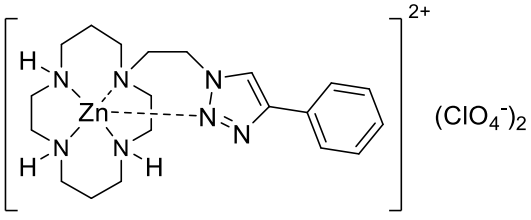

Ligand **7** (42 mg, 0.11 mmol) was complexed with $Zn(ClO_4)_2 \cdot 6H_2O$ (46 mg, 0.12 mmol) at rt using general synthetic procedure E to afford zinc complex **5** as an off-white solid (41 mg, 57%). **m.p.**: 173 ºC (decomp.). **LRMS** (ESI+): m/z 217.5 ($[M–2ClO4]^{2+}$, 100%), 375.2 (($[M–Hg–2ClO_4+H]^+$, 73%), 434.1 ($[M–2ClO_4–H]^+$, 43%), 470.2 ($[M–2ClO_4+Cl]^+$, 21%), 534.1 ($[M–ClO_4]^+$, 45%); **LRMS** (MALDI-TOF, α-CCA): *m/z* 534.2 ($[M–ClO_4]^+$, 100%); **LRMS**

(MALDI-TOF, THAP + dibasic ammonium citrate): *m/z* 626.2 ([M–2ClO_4+citrate$^-$]$^+$. **HRMS** (ESI+): *m/z* Calcd. for $C_{20}H_{33}ClN_7O_4Zn^+$ [M–ClO_4]$^+$ 534.1569, found 534.1572. **FTIR** (ATR) ν_{max}/cm^{-1}: 3236, 2879, 1456, 1066, 1000, 978, 929, 886, 848, 770, 740, 697, 620, 508.

Tri-tert-butyl 11-((1-phenyl-1H-1,2,3-triazol-4-yl)methyl)-1,4,8,11-tetraazacyclotetradecane-1,4,8-tricarboxylate ***14***

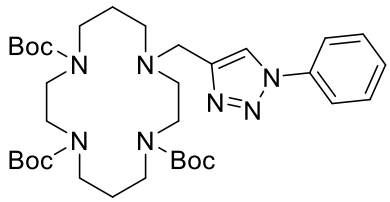

Tri-Boc-propargylcyclam **11** (379 mg, 0.67 mmol) and phenyl azide (102 mg, 1.00 mmol) were reacted using general synthetic procedure **A** and purified by automated flash column chromatography (10 g cartridge, 12% EtOAc in P.E. over 1 CV, 12 to 100% over 10 CV and 100% over 1 CV) to afford click product **14** as an off-white foam (385 mg, 88%). **^{1}H NMR** ($CDCl_3$, 500 MHz): δ 1.41 (s, 9H), 1.44 (s, 18H), 1.75 (qn, 2H, *J* 6.3), 1.86 – 1.97 (m, 2H), 2.46 – 2.55 (m, 2H), 2.62 – 2.71 (m, 2H), 3.23 – 3.52 (m, 12H), 3.87 (s, 2H), 7.40 – 7.46ma (m, 1H), 7.49 – 7.56 (m, 2H), 7.77 (d, 2H, *J* 7.8), 7.82 – 8.03 (m, 1H). **^{13}C NMR** ($CDCl_3$, 100 MHz): δ 26.7, 28.5, 28.5, 28.5, 45.6, 47.7, 49, 51.2, 79.6, 120.5, 128.6, 129.7, 137.1, 155.9. **LRMS** (ESI+): *m/z* 658.5 ([M+H]$^+$, 23%), 680.4 ([M+Na]$^+$, 100%). **HRMS** (ESI+): *m/z* Calcd. for $C_{34}H_{56}N_7O_6^+$ [M+H]$^+$ 658.4287, found 658.4288. **FTIR** (ATR) ν_{max}/cm^{-1}: 2975, 2932, 1684, 1503, 1478, 1414, 1366, 1245, 1163, 1043, 761, 732.

1-((1-Phenyl-1H-1,2,3-triazol-4-yl)methyl)-1,4,8,11-tetraazacyclotetradecane ***8***

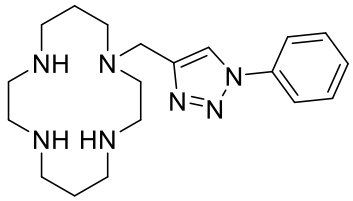

Protected ligand **14** (110 mg, 0.12 mmol) was deprotected using general synthetic procedure C to afford Boc deprotected **8** as a sticky off-white solid (60 mg, 100%). **^{1}H NMR** (DMSO-d_6, 500 MHz): δ 1.51 – 1.64 (m, 2H), 1.71 – 1.82 (m, 2H), 2.46 (t, 2H, *J* 5.5), 2.48 – 2.55 (m, 2H), 2.55 – 2.74 (m, 12H), 3.83 (s, 2H), 7.48 (t, 1H, *J* 7.4), 7.60 (t, 2H, *J* 7.9), 7.89 (d, 2H, *J* 7.6), 8.69 (s, 1H). **^{13}C NMR** (DMSO-d_6, 125 MHz): δ 25.4, 27.8, 45.9, 46.5, 47.2, 47.8, 48, 49.4, 50.6, 53.3, 56, 62.8, 119.9, 121.9, 128.5, 129.9, 136.7, 143.3. **LRMS** (ESI+): *m/z* 358.2

([M+H]$^+$, 100%). **HRMS** (ESI+): *m/z* Calcd. for $C_{19}H_{31}N_7Na^+$ 380.2533, found 380.2533. **FTIR** (ATR) ν_{max}/cm^{-1}: 2975, 2932, 1687, 1502, 1478, 1465, 1414, 1391, 1366, 1296, 1246, 1164, 861, 761, 733, 688.

Mercury perchlorate complex of 1-((1-phenyl-1H-1,2,3-triazol-4-yl)methyl)-1,4,8,11-tetraaza-cyclotetradecane ***6***

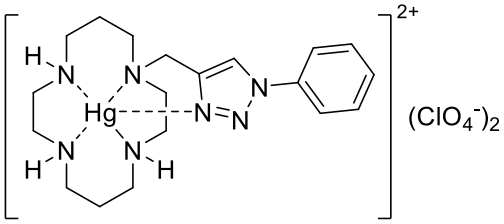

Ligand **8** (50 mg, 0.14 mmol) was complexed with $Hg(ClO_4)_2{\cdot}4H_2O$ (73 mg, 0.16 mmol) at rt using general synthetic procedure E to afford mercury complex **6** as a white solid (87 mg, 75%). **m.p.**: 190 ºC (decomp.). **LRMS** (ESI+): m/z 279.5 ([M–2ClO4]$^{2+}$, 60%), 594.1 ([M–2ClO$_4$+Cl]$^+$, 100%). **LRMS** (MALDI-TOF, α-CCA): m/z 558.3 ([M–2ClO4–H]$^+$, 100%), 658.2 ([M–ClO4]$^+$, 41%). **HRMS** (ESI$^+$): *m/z* Calcd. for $C_{19}H_{31}ClHgN_7O4^+$ [M–ClO4]$^+$ 658.1827, found 658.1827. **FTIR** (ATR) ν_{max}/cm^{-1}: 3266, 1502, 1468, 1451, 1426, 1260, 1200, 1076, 1028, 944, 929, 886, 870, 852, 768, 693, 621, 532.

Tri-tert-butyl 11-(2-(4-phenyl-1H-1,2,3-triazol-1-yl-5-d)ethyl)-1,4,8,11-tetraazacyclotetra-decane-1,4,8-tricarboxylate ***15***

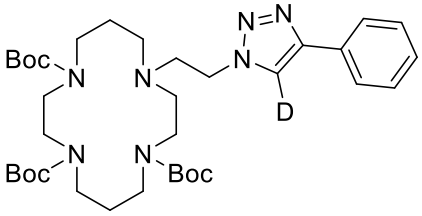

Tri-Boc-azidoethylcyclam **10** (515 mg, 0.904 mmol) and phenylacetylene (119 µL, 1.09 mmol) were reacted using modified general synthetic procedure A (temperature = rt and H_2O replaced by D_2O) and purified by flash column chromatography (EtOAc: P.E. = 2:3 to 9:1) to afford click product **15** as a white foam (495 mg, 81%). **^{1}H NMR** ($CDCl_3$, 400 MHz): δ 1.43 (s, 9H), 1.45 (s, 18H), 1.61 – 1.78 (m, 4H), 2.46 – 2.55 (m, 2H), 2.62 – 2.73 (m, 2H), 2.97 (t, 2H, *J* 6.5), 3.09 – 3.38 (m, 12H), 4.41 (t, 2H, *J* 6.5), 7.29 – 7.35 (m, 1H), 7.38 – 7.45 (m, 2H), 7.80 – 7.85 (m, 2H). **^{13}C NMR** ($CDCl_3$, 100 MHz): δ 26.5, 28.4, 28.5, 28.5, 28.8, 45.8, 46.8, 47.3, 47.7, 48.3, 52.3, 53.6, 55.1, 79.7, 79.8 120.1 (t, $J_{C\text{-}D}$ 25.9), 125.6, 128.1, 128.8, 130.6,

147.4, 155.5, 155.6, 155.7. **LRMS** (ESI+): *m/z* 673.1 ($[M+H]^+$, 62%), 695.1 ($[M+Na]^+$, 100%). **HRMS** (ESI+): *m/z* Calcd. for $C_{35}H_{56}DN_7NaO_6^+$ $[M+Na]^+$ 695.4322, found 695.4325. **FTIR** (ATR) ν_{max}/cm^{-1}: 2976, 2932, 1677, 1462, 1413, 1365, 1246, 1155, 1072, 1027, 911, 861, 775, 727, 695, 646.

*1-(2-(4-Phenyl-1H-1,2,3-triazol-1-yl-5-d)ethyl)-1,4,8,11-tetraazacyclotetradecane **17***

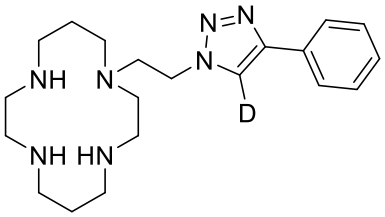

Protected ligand **15** (475 mg, 0.706 mmol) was deprotected using general synthetic procedure C to afford Boc deprotected **17** as a hygroscopic beige solid (175 mg, 67%). **^{1}H NMR** (D_2O, 500 MHz): δ 1.44 – 1.54 (m, 2H), 1.54 – 1.61 (m, 2H), 2.09 (t, 2H, *J* 6.4), 2.20 (t, 2H, *J* 5.6), 2.26 – 2.63 (m, 2H), 2.63 – 2.38 (m, 2H), 2.44 (t, 2H, *J* 5.8), 2.53 (t, 2H, *J* 5.8), 2.56 – 2.66 (m, 4H), 2.90 (t, 2H, *J* 5.5), *J* 4.52 (t, 2H, *J* 5.5), 7.43 – 7.48 (m, 1H), 7.51 – 7.56 (m, 2H), 7.80 – 7.84 (m, 2H). **^{2}H NMR** (H_2O, 61 MHz): 8.47 (br s). **^{13}C NMR** (D_2O, 125 MHz): δ 25.7, 26.6, 44.1, 44.9, 45.1, 45.6, 45.8, 46.3, 48.4, 50, 52.1, 52.5, 123.1, 125.7, 125.7, 129.2, 129.6, 129.6, 129.7, 147.3. **LRMS** (ESI+): *m/z* 373.3 ($[M+H]^+$, 100%). **HRMS** (ESI+): *m/z* Calcd. for $C_{20}H_{33}DN_7^+$ $[M+H]^+$ 373.2933, found 373.2937. **FTIR** (ATR) ν_{max}/cm^{-1}: 2944, 2821, 1462, 1360, 1286, 1224, 1123, 1073, 1049, 778, 728, 697.

*Mercury perchlorate complex of 1-(2-(4-phenyl-1H-1,2,3-triazol-1-yl-5-d)ethyl)-1,4,8,11-tetraazacyclotetradecane **19***

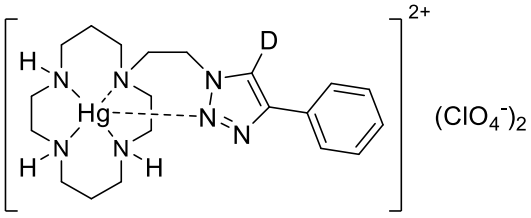

Ligand **17** (55 mg, 0.15 mmol) was complexed with $Hg(ClO_4)_2 \cdot 4H_2O$ (74 mg, 0.16 mmol) at rt using general synthetic procedure E to afford mercury complex **19** as a hygroscopic white solid (39 mg, 34%). **^{2}H NMR** (H_2O, 61 MHz): 8.68 (br s). **LRMS** (ESI+): m/z 279.9 ($[M–2ClO_4]^{2+}$, 100%), 658.9 ($[M–ClO_4]^+$, 16%). **HRMS** (ESI+): *m/z* Calcd. for

$C_{20}H_{32}DClHgN_7O_4^+$ $[M–ClO_4]^+$ 673.2048, found 673.2046. **FTIR** (ATR) ν_{max}/cm^{-1}: 3264, 2872, 1453, 1081, 930, 884, 778, 730, 699, 622.

Tri-tert-butyl 11-((1-phenyl-1H-1,2,3-triazol-4-yl-5-d)methyl)-1,4,8,11-tetraazacyclotetradecane-1,4,8-tricarboxylate ***16***

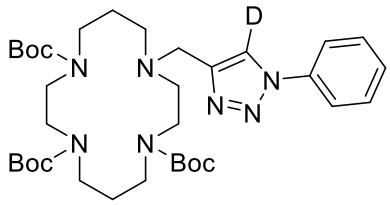

Tri-Boc-propargylcyclam **11** (320 mg, 0.594 mmol) and phenyl azide (85 mg, 0.71 mmol) were reacted using modified general synthetic procedure A (temperature = rt and H_2O replaced by D_2O) and purified by flash column chromatography (EtOAc: P.E. = 3:2) to afford click product **16** as an off-white foam (305 mg, 78%). **^{1}H NMR** ($CDCl_3$, 400 MHz): δ 1.40 (s, 9H), 1.44 (s, 18H), 1.68 – 1.81 (m, 2H), 1.84 – 1.98 (m, 2H), 2.45 – 2.55 (m, 2H), 2.63 – 2.71 (m, 2H), 3.25 – 3.50 (m, 12H), 3.86 (s, 2H), 7.39 – 7.46 (m, 1H), 7.48 – 7.56 (m, 2H), 7.76 (d, 2H, *J* 7.8). **^{13}C NMR** ($CDCl_3$, 100 MHz): δ 26.6, 27, 28.4, 28.5, 28.5, 45.5, 47.2, 48.9, 51.3, 52.1, 53, 79.6, 120.5, 128.6, 129.7, 137.1, 144.2, 155.5, 155.8. **LRMS** (ESI+): *m/z* 659.2 ($[M+H]^+$, 96%), 681.1 ($[M+Na]^+$, 100%). **HRMS** (ESI+): *m/z* Calcd. for $C_{34}H_{55}DN_7O_6^+$ $[M+H]^+$ 659.4349, found 695.4344. **FTIR** (ATR) ν_{max}/cm^{-1}: 2975, 2932, 1687, 1478, 1465, 1414, 1366, 1246, 1164, 984, 861, 761, 733, 688.

1-((1-Phenyl-1H-1,2,3-triazol-4-yl-5-d)methyl)-1,4,8,11-tetraazacyclotetradecane ***18***

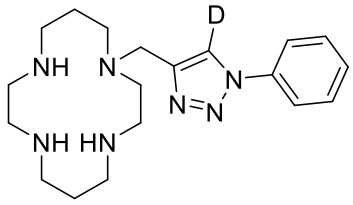

Protected ligand **16** (290 mg, 0.440 mmol) was deprotected using general synthetic procedure C to afford Boc deprotected **18** as a sticky off-white solid (158 mg, 100%). **^{1}H NMR** (D_2O, 500 MHz): δ 1.75 – 1.83 (m, 2H), 1.98 – 2.06 (m, 2H), 2.72 – 2.77 (m, 2H), 2.79 (t, 2H, *J* 5.4), 2.87 – 2.96 (m, 4H), 2.98 – 3.07 (m, 6H), 3.08 (t, 2H, *J* 5.1), 3.90 (s, 2H), 7.57 – 7.63 (m, 1H), 7.57 – 7.69 (m, 2H), 7.76 – 7.81 (m, 2H). **^{13}C NMR** (D_2O, 125 MHz): δ 23.7, 25.6, 45.6, 45.7, 46.4, 47.4, 48, 49.2, 49.5, 50, 52.7, 54.1, 121.4, 123.6, 129.9, 130.3, 136.6, 144.6.

LRMS (ESI+): *m/z* 359.1 ([M+H]$^+$, 100%). **HRMS** (ESI+): *m/z* Calcd. for $C_{19}H_{31}DN_7$+ [M+H]$^+$ 359.2777, found 359.2777. **FTIR** (ATR) ν_{max}/cm^{-1}: 2946, 2834, 1597, 1500, 1463, 1340, 1226, 1114, 1050, 982, 855, 761, 688, 516.

*Mercury perchlorate complex of 1-((1-phenyl-1H-1,2,3-triazol-4-yl-5-d)methyl)-1,4,8,11-tetraazacyclotetradecane **20***

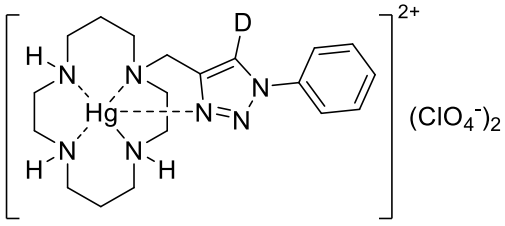

Ligand **18** (65 mg, 0.18 mmol) was complexed with $Hg(ClO_4)_2 \cdot 4H_2O$ (94 mg, 0.20 mmol) at rt using general synthetic procedure E to afford mercury complex **20** as a hygroscopic white solid (43 mg, 31%). **LRMS** (ESI+): m/z 595.0 ([M–2ClO$_4$+Cl]$^+$, 100%). **FTIR** (ATR) ν_{max}/cm^{-1}: 3549, 3272, 2863, 1597, 1500, 1463, 1428, 1068, 986, 931, 916, 863, 763, 688, 621, 517. **HRMS** (ESI+): *m/z* Calcd. for $C_{19}H_{30}DClHgN_7$+ [M–2ClO$_4$+Cl]$^+$ 595.2095, found 595.2094.

NMR Titrations

To a solution of the *substituted cyclam* (0.5 mL, 2.5 mM in D_2O) in an NMR tube were added sequential aliquots of the *salt/ competing ligand* solution (250 mM in D_2O) to deliver 1, 2, 5, 10, 20 and then 100 molar equivalents. Solutions were shaken for 2 minutes to ensure complete mixing before spectra were recorded; spectra were calibrated to the residual proton solvent peak in D_2O (4.79 ppm).

Acknowledgements

We thank the Australian Research Council (DP120104035) and the National Health and Medical Research Council (APP1084266) for funding. J. K.-H.Wong was supported by an Australian Postgraduate Award (APA) from the Australian Government.

References

[1] S. M. Cohen, *ChemMedChem* **2014**, *9*, 1087-1089.
[2] N. P. E. Barry, P. J. Sadler, *ACS Nano* **2013**, *7*, 5654-5659.
[3] C.-M. Che, F.-M. Siu, *Curr. Opin. Chem. Biol.* **2010**, *14*, 255-261.
[4] S. Medici, M. Peana, V. M. Nurchi, J. I. Lachowicz, G. Crisponi, M. A. Zoroddu, *Coord. Chem. Rev.* **2015**, *284*, 329-350.

[5] G. Gasser, *Chimia* **2015**, *69*, 442-446.
[6] G. Colotti, A. Ilari, A. Boffi, V. Morea, *Mini-Rev. Med. Chem.* **2016**, *13*, 211-221.
[7] P. C. A. Bruijnincx, P. J. Sadler, *Curr. Opin. Chem. Biol.* **2008**, *12*, 197-206.
[8] E. Tamanini, S. E. J. Rigby, M. Motevalli, M. H. Todd, M. Watkinson, *Chem. Eur. J.* **2009**, *15*, 3720-3728.
[9] M. Yu, Q. Yu, P. J. Rutledge, M. H. Todd, *ChemBioChem* **2013**, *14*, 224-229.
[10] Y. H. Lau, J. R. Price, M. H. Todd, P. J. Rutledge, *Chem. Eur. J.* **2011**, *17*, 2850-2858.
[11] E. Tamanini, A. Katewa, L. M. Sedger, M. H. Todd, M. Watkinson, *Inorg. Chem.* **2009**, *48*, 319-324.
[12] S. Ast, P. J. Rutledge, M. H. Todd, *Eur. J. Inorg. Chem.* **2012**, *2012*, 5611-5615.
[13] M. Yu, J. K.-H. Wong, C. Tang, P. Turner, M. H. Todd, P. J. Rutledge, *Beilstein J. Org. Chem.* **2015**, *11*, 37-41.
[14] M. Yu, S. Ast, Q. Yu, A. T. S. Lo, R. Flehr, M. H. Todd, P. J. Rutledge, *PLoS ONE* **2014**, *9*, e100761.
[15] M. Yu, T. M. Ryan, S. Ellis, A. I. Bush, J. A. Triccas, P. J. Rutledge, M. H. Todd, *Metallomics* **2014**, *6*, 1931-1940.
[16] J. K.-H. Wong, S. Ast, M. Yu, R. Flehr, A. J. Counsell, P. Turner, P. Crisologo, M. H. Todd, P. J. Rutledge, *ChemistryOpen* **2016**, DOI: 10.1002/open.201600010.
[17] M. Yu, J. R. Price, P. Jensen, C. J. Lovitt, T. Shelper, S. Duffy, L. C. Windus, V. M. Avery, P. J. Rutledge, M. H. Todd, *Inorg Chem* **2011**, *50*, 12823-12835.
[18] M. Yu, N. H. Lim, S. Ellis, H. Nagase, J. A. Triccas, P. J. Rutledge, M. H. Todd, *ChemistryOpen* **2013**, *2*, 99-105.
[19] M. Yu, G. Nagalingam, S. Ellis, E. Martinez, V. Sintchenko, M. Spain, P. J. Rutledge, M. H. Todd, J. A. Triccas, *J. Med. Chem.* **2016**, *59*, 5917-5921.
[20] L. Jin, D. R. Tolentino, M. Melaimi, G. Bertrand, *Sci. Adv.* **2015**, *1*, e1500304.
[21] H. K. Akula, M. K. Lakshman, *J. Org. Chem.* **2012**, *77*, 8896-8904.
[22] B. Bosnich, C. K. Poon, M. L. Tobe, *Inorg. Chem.* **1965**, *4*, 1102-1108.
[23] R. B. Martin, in *Encyclopedia of Inorganic Chemistry* (Ed.: R. B. King), John Wiley & Sons, Ltd, **2006**.
[24] J. Burgess, R. H. Prince, in *Encyclopedia of Inorganic Chemistry* (Ed.: R. B. King), John Wiley & Sons, Ltd, **2006**.
[25] R. Colton, D. Dakternieks, *Inorg. Chim. Acta* **1993**, *208*, 173-177.
[26] B. T. Worrell, J. E. Hein, V. V. Fokin, *Angew. Chem. Int. Ed.* **2012**, *51*, 11791-11794.
[27] P. A. Champagne, J. Desroches, J.-D. Hamel, M. Vandamme, J.-F. Paquin, *Chem. Rev.* **2015**, *115*, 9073-9174.